Mathematical Biosciences and Engineering

http://www.aimspress.com/journal/mbe

MBE, 19(9): 8689–8704.
DOI: 10.3934/mbe.2022403
Received: 31 December 2021
Revised: 19 May 2022
Accepted: 09 June 2022
Published: 16 June 2022

Research article

The force of cell-cell adhesion in determining the outcome in a nonlocal advection diffusion model of wound healing

Glenn Webb*

Mathematics Department, Vanderbilt University, Nashville, TN, USA

* **Correspondence:** Email: glenn.f.webb@vanderibilt.edu; Tel: +16153226661.

Abstract: A model of wound healing is presented to investigate the connection of the force of cell-cell adhesion to the sensing radius of cells in their spatial environment. The model consists of a partial differential equation with nonlocal advection and diffusion terms, describing the movement of cells in a spatial environment. The model is applied to biological wound healing experiments to understand incomplete wound closure. The analysis demonstrates that for each value of the force of adhesion parameter, there is a critical value of the sensing radius above which complete wound healing does not occur.

Keywords: nonlocal; advection; diffusion; adhesion; wound healing experiment

1. Introduction

The movement of cells in spatial micro-environments can be modeled by continuous variables for the continuum density of the cells. The partial differential equations of these models incorporate two components of cell movement: diffusion corresponding to random motion and nonlocal advection corresponding to directed motion. In this work we employ nonlocal advection diffusion models to describe the movement of biological cells in wound healing experiments. In these experiments, cells have a directed motion corresponding to cell-cell adhesion. Cell-cell adhesion is a fundamental feature of multi-cellular organisms, and is linked to maintenance of order in tissue formation, stability, and breakdown.

There are several signaling pathways that control normal cell processes, such as cell proliferation, cell division, cellular adhesion, and apoptosis. One of the most important signaling pathways is transforming growth factor beta $TGF\beta$, which regulates the proliferation, differentiation, adhesion, migration, and apoptosis of many cell types, including endothelial cells, hematopoietic cells, lymphocytes, and ECM production.

In wound healing experiments, cells lie in a viscous thin layer in a laboratory well, and are subjected to experimental drug therapies. Cells in the layer are moving and proliferating. The velocity of a cell is proportional to the net adhesive force acting on it, due to bonds formed with nearby cells. This adhesive flux results, because cells sense their surroundings over a sensing radius via protrusions such as filopodia, which interact with nearby cells to facilitate intercellular communication. The sensing radius is considerable larger than the cell radius. The division of cells depends on a nutrient furnished to the cell population. In the experiments, the layer of cells is scored laterally to form a narrow depression, which then restores completely to the original level layer, or incompletely to a series of ridges.

In our references we have cited works that treat laboratory wound healing experiments [1–10]. In Figure 1, images from wound healing experiments in [4] are given. In these experiments, human umbilical vein endothelial cells were plated on gelatin-coated plastic dishes and wounded with a pipette tip, and then imaged by microscope over several hours.

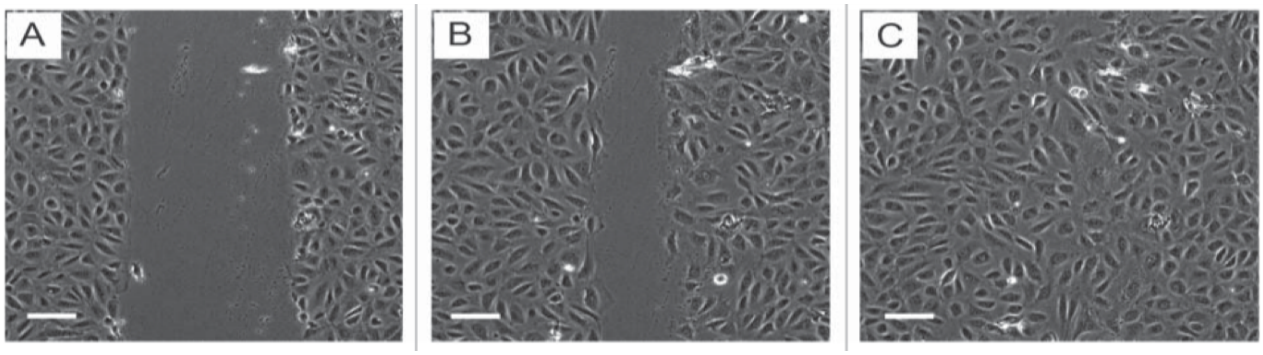

Figure 1. Images of wound healing assays at three different time points for experiments in a human umbilical vein endothelial cell monolayer in [4]. The bars are length 120 μm. The experiment images are 15 minutes apart.

In [11], numerical simulations were given to investigate the dependence of wound closure on the diffusion parameter α. In this work, our objective is to examine the relationship in (2.1), between the sensing radius ρ and the adhesive force parameter λ in $g(n) = n(\lambda - n)$. We will demonstrate numerically, that this relationship depends on ρ and λ in such a way that for λ sufficiently large, there is a critical value $\rho_c(\lambda)$ of ρ such that $n(x,t)$ converges to $\bar{n}(x)$ for ρ less than $\rho_c(\lambda)$. For ρ greater than $\rho_c(\lambda)$, $n(x,t)$ does not converge to $\bar{n}(x)$, and incomplete closure occurs, with a series of ridges established above and below $\bar{n}(x)$. We will also examine the spacing $\rho_s(\lambda)$ of the spatial ridges in the case of incomplete wound closure, as a function of λ.

2. Nonlocal advection diffusion model applied to wound healing experiments

In our references we have cited works that treat laboratory wound healing experiments with mathematical models [2, 10–65]. We note in particular the nonlocal advection diffusion models of wound healing experiments by Stephen Gourley [11, 25, 56]. In [11], the partial differential equation of the nonlocal advection diffusion model for wound healing has the following form:

$$\frac{\partial n(x,t)}{\partial t} = \underbrace{\alpha \frac{\partial^2 n(x,t)}{\partial x^2}}_{\text{random motility}} - \underbrace{\frac{\partial}{\partial x}\left(n(x,t)\int_{-\rho}^{\rho} g(n(x+\hat{x},t))\,h(\hat{x})\,d\hat{x}\right)}_{\text{cell-cell adhesion}} + \underbrace{f(n(x,t))}_{\text{cell loss and gain}}, \quad n(x,0) = n_0(x), \quad (2.1)$$

where x is spatial position, $-\infty < x < \infty$, and t is time, $t \geq 0$.

The model in [17] for cell-cell adhesion has a direct representation of cell-cell contact using a nonlocal spatial term in the model equation. This formulation was originally due to Armstrong, Painter, and Sherratt [13], and subsequently applied to somite formation in early vertebrate development (Armstrong, Painter, and Sherratt [14]), to tumour growth (Gerisch and Chaplain [39]), and to cancer invasion (Sherratt, Gourley, Armstrong, and Painter [56]). These authors considered basic properties of the models, such as positivity, boundedness, and spatial pattern formation, which are important for biological applications.

In (2.1), $n(x,t)$ is the 1-dimensional continuum density of cells with respect to the lateral position x across the wound at time t. The initial condition $n(x,0) = n_0(x)$ corresponds to the wound depth at spatial position x at time 0. The domain of $n(x,t)$ is taken as $(-\infty,\infty)$, since the boundary of the laboratory well is not significant compared to the sensing radius. The interpretation of the model outcomes relates to early or intermediate dynamics over time, which are not influenced by cells near the boundary of the laboratory well.

In (2.1), α is the diffusion constant, g describes the advection force on a cell at position x due to other cells within a sensing radius ρ centered at x, h describes variation of the advection force over the sensing radius centered at x, and f describes the loss or gain of cells at position x. The sensing radius quantifies the total forces attributable to bonds formed by cells at nearby locations due to cell protrusions such as filopodia. The magnitude of these local forces depends on the number of attachments made by cells within the experimentally specified sensing radius.

In (2.1), $\int_{-\rho}^{\rho} g(n(x+\hat{x},t)\,h(\hat{x})\,d\hat{x}$ represents the total adhesive force, attributable to cell-cell bonding, on a cell at position x from cells at position $x+\hat{x}$, $\hat{x} \in (x-\rho, x+\rho)$. The function $g(n)$ is approximately linear for small n, decreases for n above some threshold, and is effectively 0 above some critical value. In our numerical simulations of (2.1), we will assume that $g(n) = n(\lambda - n)$ with $\lambda > 1$. We will call λ the cell-cell adhesion constant.

The function $h(\hat{x})$ in (2.1) represents the magnitude and direction of the adhesive force over the sensing radius of the cell as a function of $\hat{x} \in (-\rho, \rho)$. This force diminishes with increasing separation of cells. The adhesive force is directed towards cell centers. The force on a cell at x due to a cell at $x+\xi$ will tend to pull the cell at x to the right if $\xi > 0$, and to the left if $\xi < 0$. The direction of the adhesive force, toward the cell at position x, requires $h(\hat{x})$ to be an odd function, with $\hat{x} \geq 0$ for $\hat{x} \geq 0$. In our numerical simulations, we will take $h(\hat{x}) = 0.1 \arctan(0.2\,\hat{x})/\arctan(0.2)$. The function $f(n)$ in (2.1) is of logistic type, so that at lower cell densities, there is increased cell division, and at higher cell densities there is cell loss due to overcrowding. In our simulations, we will take $f(n) = n(1-n)$, corresponding to a normalization of the density at the equilibrium value $\bar{n}(x) \equiv 1$.

In [11], the existence, regularity, positivity, boundedness, and asymptotic behavior of the solutions of (2.1) was investigated with the above assumptions. In [25], the model was extended to higher dimensional spatial domains for the cell densities. In [30], the model was extended to include proliferating cell age structure corresponding to the cell cycle. In [30], operator semigroup methods were

used to establish suffucient conditions for the local asymptotic stability of the wound free equilibrium. In [11], the following sufficiency result was proven for the global asymptotic stability of the equilibrium $\bar{n}(x) \equiv 1$ in the model (2.1):

Theorem. Let h be an odd function such that $h(\xi) \geq 0$ when $\xi \geq 0$, let $f(n) = n(1-n)$, and let $g(n) = n(\lambda - n)$ with $\lambda > 1$. Suppose that $\delta < n_0(x) \leq \lambda$ for all $x \in R$, where $\delta > 0$. Suppose

$$\frac{\lambda^2}{4\alpha}\left(\max(1, \lambda - 1)\int_{-\rho}^{\rho} |h(\xi)|\, d\xi\right)^2 < \delta,$$

$$\frac{\lambda^2}{4}\int_{-\rho}^{\rho} |h'(\xi)|\, d\xi + \frac{h(\rho)\lambda^2}{2} < 1 - \delta,$$

$$1 + \frac{\lambda^2}{4}\int_{-\rho}^{\rho} |h'(\xi)|\, d\xi < \lambda.$$

Then, $n(x,t)$ converges to 1 as $t \to \infty$, exponentially in $L^2(R)$.

In general, the result is sufficient, but not necessary for complete would healing.

3. Numerical simulations of the wound healing experiments

In our numerical simulations we will view cells in the laboratory well as a culture grown to confluence in nutrient medium, and then incubated in serum-free medium. Before the wound is imposed, the cell density is constant at the normalized equilibrium value $\bar{n}(x) \equiv 1$. The layer of cells is scraped with a plastic pipette tip, and then replenished with serum-free medium. The healing of the wound can be viewed as the lateral closure of the wound across the scoring. Dependent on model parameters, the proliferating cells close the wound back to the equilibrium density $\bar{n}(x)$, or form an incomplete closure consisting of a series of ridges above and below the equilibrium.

In our simulations, the diffusion parameter $\alpha = 1.0$, the initial condition is taken as $n_0(x) = 1.0 - 0.75\, e^{-(0.1x)^6}$, corresponding to the lateral depression of the cells forming the wound, centered at $x = 0$ (Figure 2), and the adhesion force magnitude function is $h(\hat{x}) = 0.1 \arctan(0.2\,\hat{x})/\arctan(2.0)$. Comparable results can be obtained for similar values of α, $n_0(x)$, and $h(\hat{x})$.

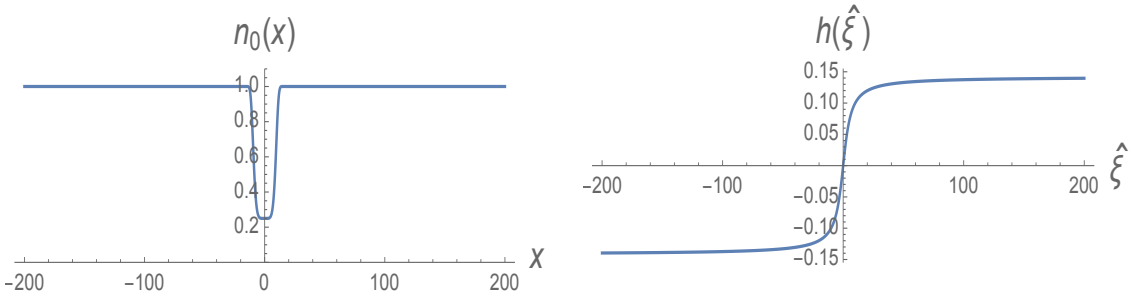

Figure 2. Left side: Graph of the initial density $n_0(x)$ of the wound at time 0. The graph represents a lateral cross section of the scored cell layer before the nutrient medium is added to promote wound healing. Right side: Graph of the intensity function $h(\hat{\xi})$ in the force of cell–cell adhesion.

With the parameters and initial condition above, we will illustrate wound closure dependence on the sensing radius ρ and the adhesion force parameter λ in the force of adhesion function $g(n) = n(\lambda - n)$. We will determine the critical value $\rho_c(\lambda)$ distinguishing complete wound closure from incomplete wound closure. We will examine the character of the spatial density function $n(x,t)$ in the case of incomplete wound closure with respect to the spacing of the oscillating spatial ridges of $n(x,t)$. We will provide three examples of λ to illustrate the critical sensing radius $\rho_c(\lambda)$ as a function of λ: $\lambda = 5.0$, $\lambda = 6.0$, and $\lambda = 7.0$.

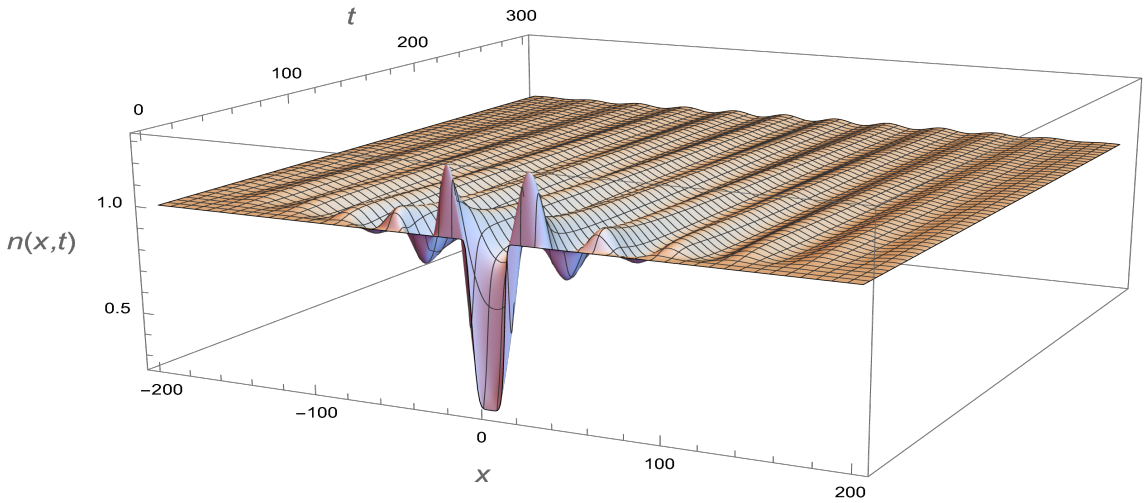

Figure 3. $\lambda = 5.0$ and $\rho = 16.9$. Graph of $n(x,t)$ for $t = 0$ to $t = 300$. The wound closes completely as t advances.

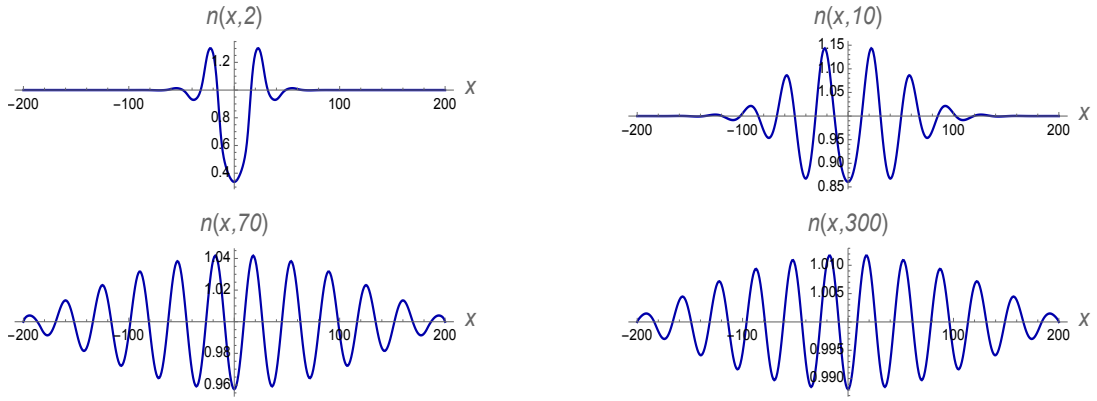

Figure 4. $\lambda = 5.0$ and $\rho = 16.9$. Graphs of $n(x,2)$, $n(x,10)$, $n(x,70)$, $n(x,300)$. The vertical axes are scaled closer to 0.0 at times 3, 10, 70, and 300, which means that the magnitude of the oscillations are decreasing as time t advances. As t advances, the maxima (and minima) of the oscillations in the x direction are spaced ≈ 38.5 units apart.

In the first simulation, $\lambda = 5.0$ and $\rho = 16.9$. The graph of $n(x,t)$ is given for time from $t = 0$ to $t = 300$ in Figure 3. In Figure 4, the $n(x,t)$ is graphed at $t = 2, t = 10, t = 70, t = 300$. As time

advances, $n(x,t)$ converges to the equilibrium $\bar{n}(x) \equiv 1.0$, and the wound closes completely. At every time level, the graph is concave up at $x = 0.0$.

In the second simulation, $\lambda = 5.0$ and $\rho = 17.0$. The graph of $n(x,t)$ is given for $t = 0$ to $t = 200$ in Figure 5. In Figure 6, $n(x,t)$ is graphed at $t = 2$, $t = 10, t = 70, t = 200$. As time advances, $n(x,t)$ does not converge to the equilibrium $\bar{n}(x) \equiv 1.0$, and the wound does not close completely. In the early dynamics, the wound stabilizes to a series of ridges with spacing ≈ 38.5. At every time level, the graph of $n(x,t)$ is concave up at $x = 0.0$. The critical value $\rho_c(\lambda)$ for $\lambda = 5.0$ is $\rho_c(5.0) \approx 17.0$. The three sufficiency conditions above for $\lim_{t\to\infty} n(x,t) = 1$, require $\rho < 1.72$ with $\delta = 0.25 = n_0(0)$.

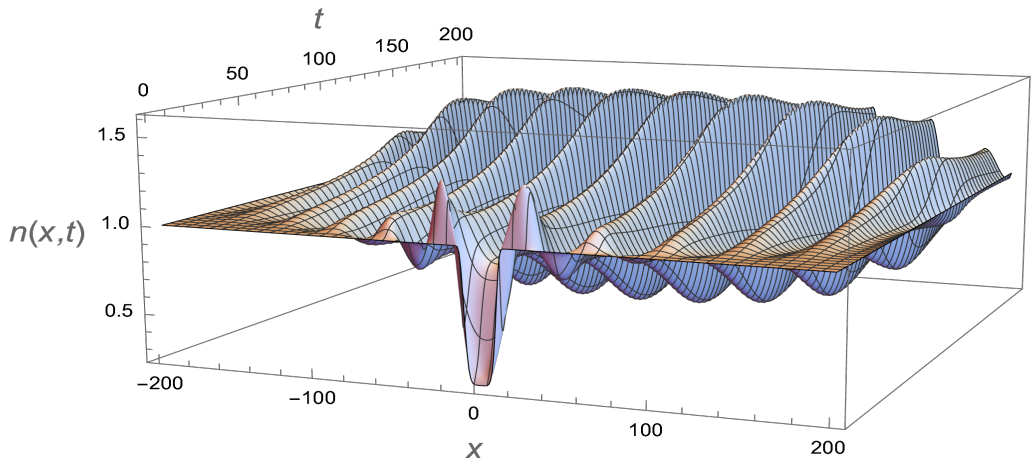

Figure 5. $\lambda = 5.0$ and $\rho = 17.0$. Graph of $n(x,t)$ for $t = 0.0$ to $t = 200$. The wound closes incompletely as t advances.

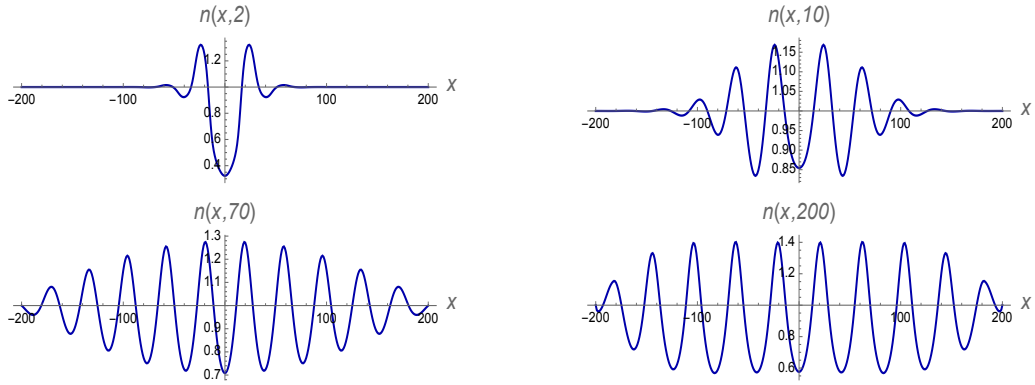

Figure 6. $\lambda = 5.0$ and $\rho = 17.0$. Graphs of $n(x,2)$, $n(x,10)$, $n(x,70)$, $n(x,200)$. As t advances, the maxima (and minima) of the oscillations in the x direction are spaced ≈ 38.5 units apart.

In the third simulation, $\lambda = 6.0$ and $\rho = 10.9$. The graph of $n(x,t)$ is given for $t = 0$ to $t = 300$ in Figure 7. In Figure 8, $n(x,t)$ is graphed at $t = 2.0$, $t = 10.0, t = 70.0, t = 300.0$. As time advances,

$n(x,t)$ converges to the equilibrium $\bar{n}(x) \equiv 1.0$, and the wound closes completely. At every positive time level, the graph is concave down at $x = 0.0$.

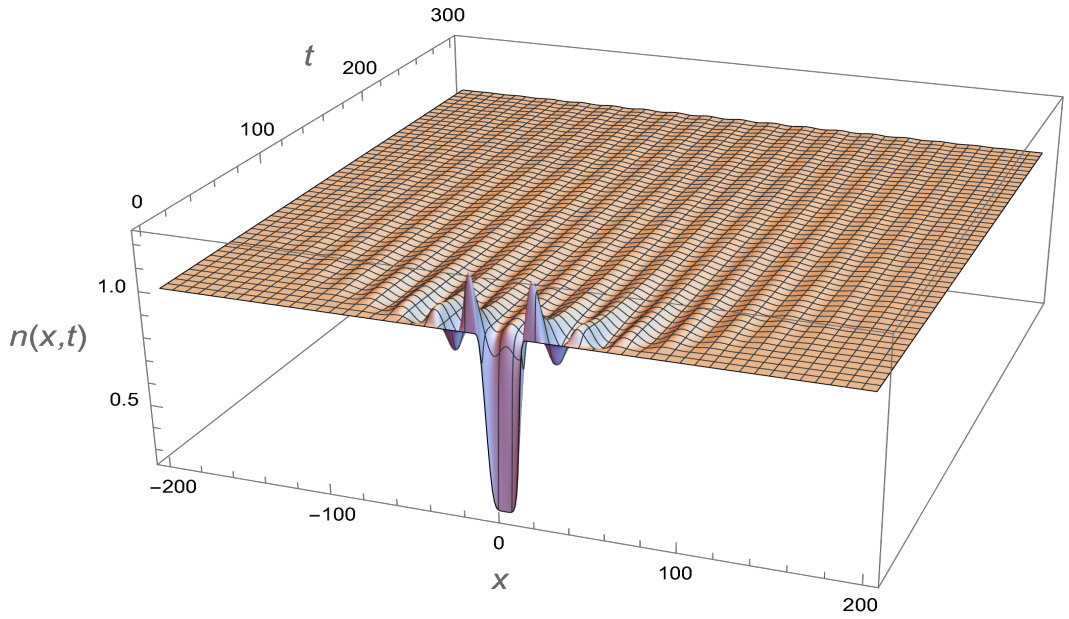

Figure 7. $\lambda = 6.0$ and $\rho = 10.9$. Graph of $n(x,t)$ for $t = 0$ to $t = 300$. The wound closes completely as t advances.

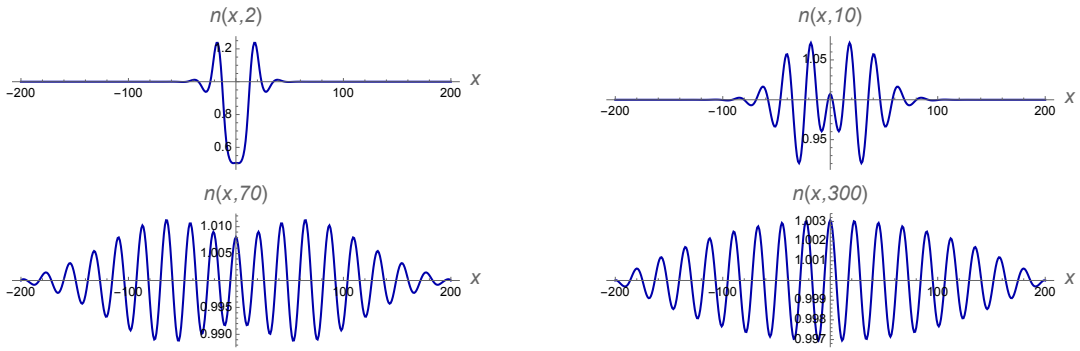

Figure 8. $\lambda = 6.0$ and $\rho = 10.9$. Graphs of $n(x,2)$, $n(x,10)$, $n(x,70)$, $n(x,300)$. As t advances, the maxima (and minima) of the oscillations in the x direction are spaced ≈ 27.8 units apart.

In the fourth simulation, $\lambda = 6.0$ and $\rho = 11.0$. The graph of $n(x,t)$ is given for $t = 0$ to $t = 300$ in Figure 9. In Figure 10, $n(x,t)$ is graphed at $t = 2.0$, $t = 10.0, t = 70.0, t = 300.0$. As time advances, $n(x,t)$ does not converge to the equilibrium $\bar{n}(x) \equiv 1.0$, and the wound does not close completely. In the early dynamics, the wound stabilizes to a series of ridges with spacing ≈ 27.8. At every time level, the graph is concave down at $x = 0.0$. The critical value $\rho_c(\lambda)$ for $\lambda = 6.0$ is $\rho_c(6.0) \approx 11.0$. The three sufficiency conditions above for $\lim_{t\to\infty} n(x,t) = 1$, require $\rho < 1.18$ with $\delta = 0.25 = n_0(0)$.

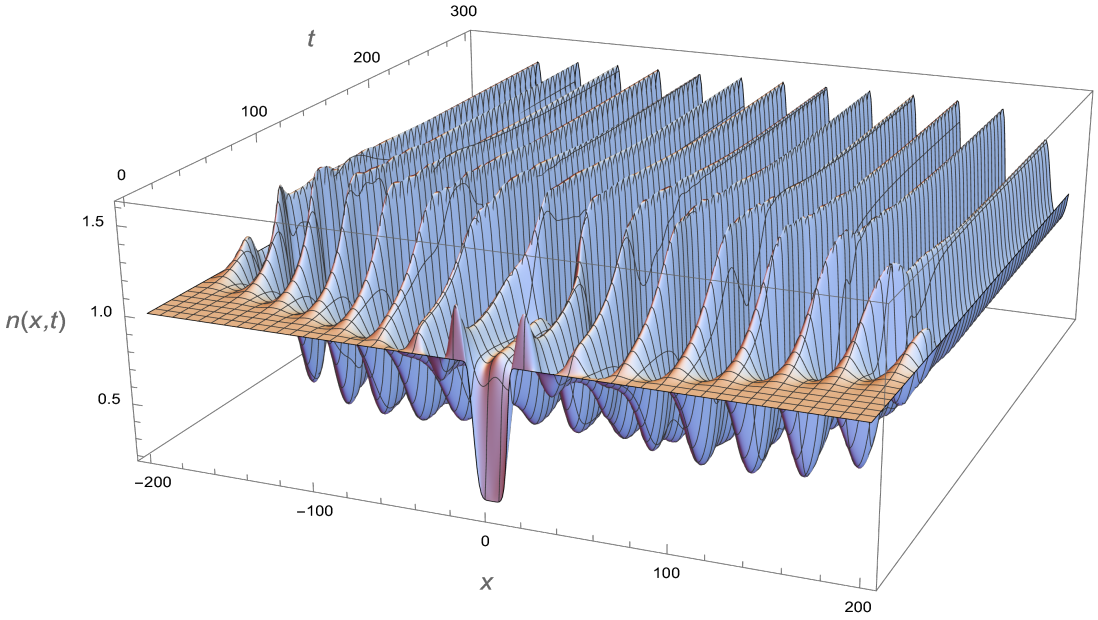

Figure 9. $\lambda = 6.0$ and $\rho = 11.0$. Graph of $n(x,t)$ for $t = 0.0$ to $t = 300$. The wound closes incompletely as t advances

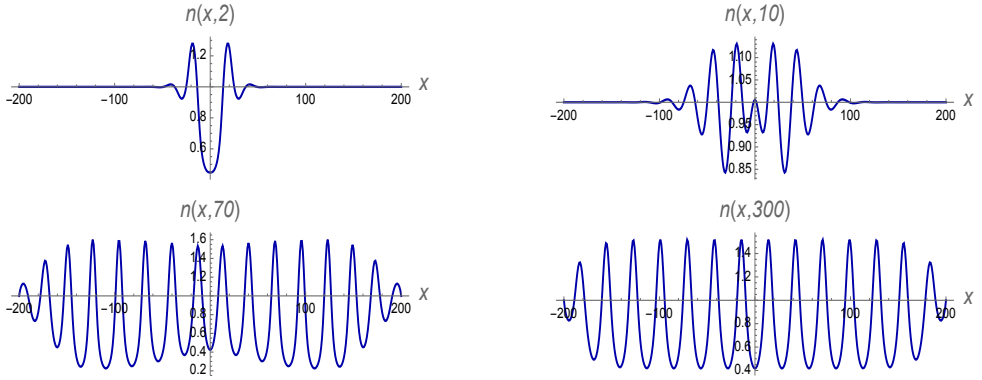

Figure 10. $\lambda = 6.0$ and $\rho = 11.0$. Graphs of $n(x,2)$, $n(x,10)$, $n(x,70)$, $n(x,300)$. As t advances, the maxima (and minima) of the oscillations in the x direction are spaced ≈ 27.8 units apart.

In the fifth simulation, $\lambda = 7.0$ and $\rho = 7.9$. The graph of $n(x,t)$ is given for time from $t = 0$ to $t = 100$ in Figure 11. In Figure 12, $n(x,t)$ is graphed at $t = 2.0$, $t = 10.0, t = 70.0, t = 100.0$. As time advances, $n(x,t)$ converges to the equilibrium $\bar{n}(x) \equiv 1.0$, and the wound closes completely. At every time level, the graph is concave down at $x = 0.0$.The critical value $\rho_c(\lambda)$ for $\lambda = 7.0$ is $\rho_c(7.0) \approx 8.0$. The three sufficiency conditions above for $\lim_{t\to\infty} n(x,t) = 1$, require $\rho < 1.9$ with $\delta = 0.25 = n_0(0)$.

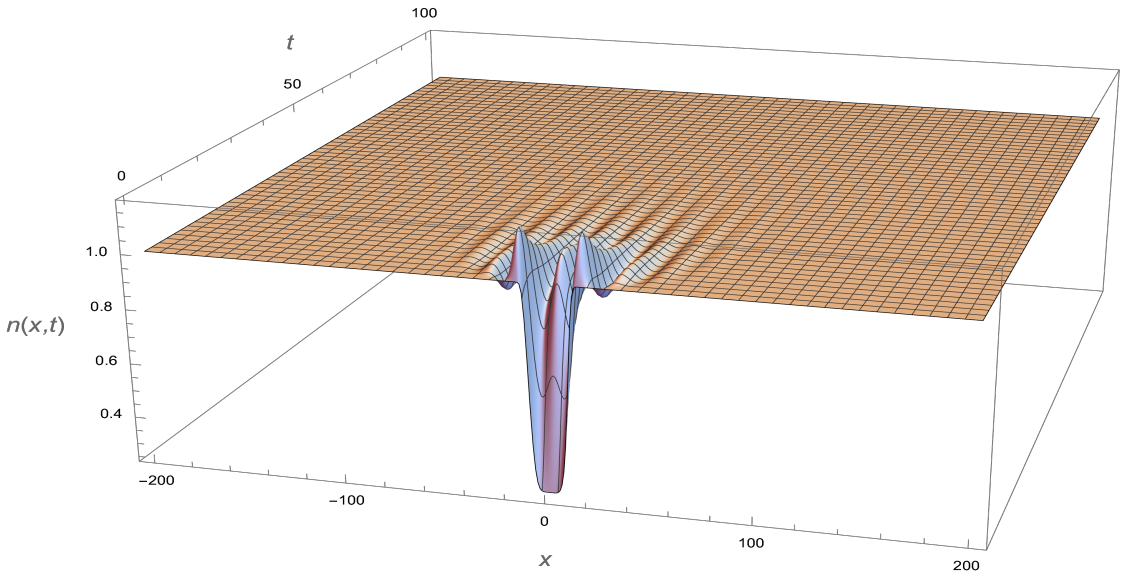

Figure 11. $\lambda = 7.0$ and $\rho = 7.9$. Graph of $n(x,t)$ for $t = 0.0$ to $t = 100$. The wound closes completely as t advances.

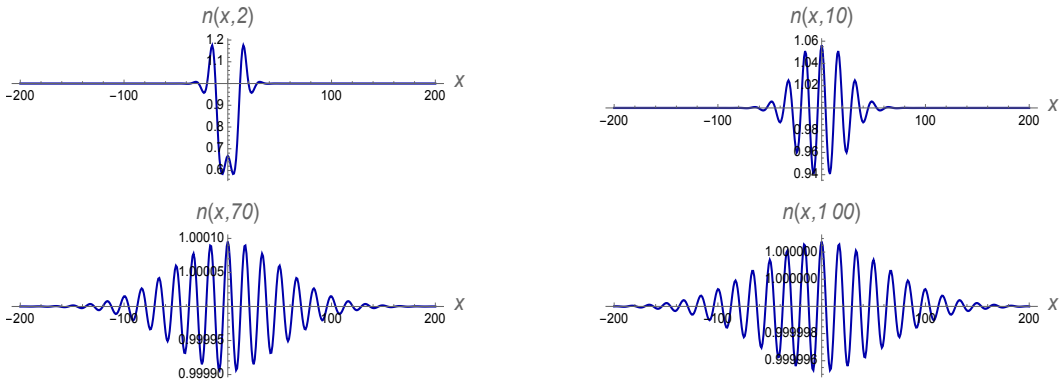

Figure 12. $\lambda = 7.0$ and $\rho = 7.9$. Graphs of $n(x,2)$, $n(x,10)$, $n(x,70)$, $n(x,100)$. As t advances, the maxima (and minima) of the oscillations in the x direction are spaced ≈ 27.8 units apart.

In the sixth simulation, $\lambda = 7.0$ and $\rho = 8.0$. The graph of $n(x,t)$ is given for time from $t = 0$ to $t = 100$ in Figure 13. In Figure 14, $n(x,t)$ is graphed at $t = 2.0$, $t = 10.0, t = 70.0, t = 100.0$. As time advances, $n(x,t)$ does not converge to the equilibrium $\bar{n}(x) \equiv 1.0$, and the wound does not close completely. In the early dynamics, the wound stabilizes to a series of ridges with spacing ≈ 20.0. At every time level, the graph is concave down at $x = 0.0$. The critical value $\rho_c(\lambda)$ for $\lambda = 7.0$ is $\rho_c(7.0) \approx 8.0$. The three sufficiency conditions above for $\lim_{t\to\infty} n(x,t) = 1$, require $\rho < 0.86$ with $\delta = 0.25 = n_0(0)$.

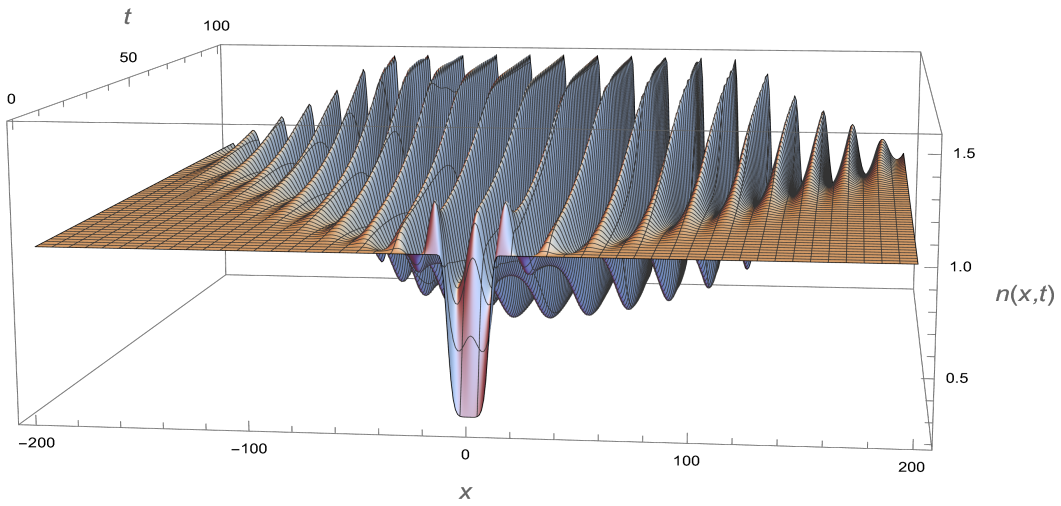

Figure 13. $\lambda = 7.0$ and $\rho = 8.0$. Graph of $n(x,t)$ for $t = 0.0$ to $t = 100$. The wound closes incompletely as t advances.

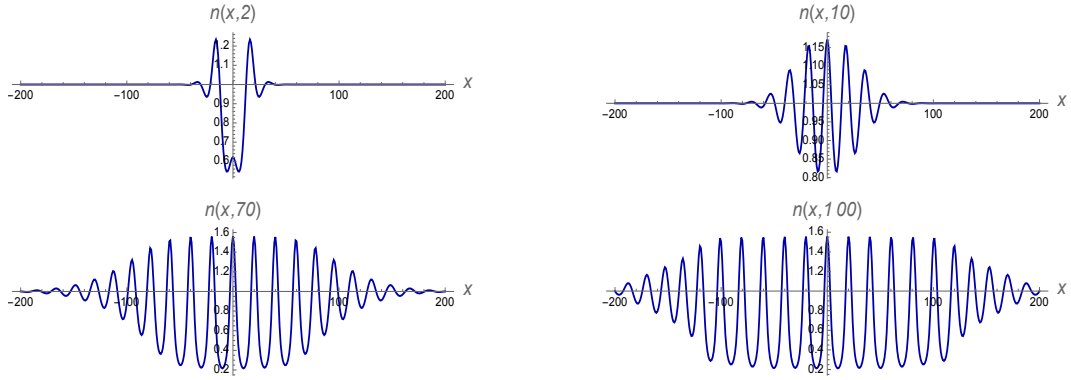

Figure 14. $\lambda = 7.0$ and $\rho = 8.0$. Graphs of $n(x,2)$, $n(x,10)$, $n(x,70)$, $n(x,100)$. As t advances, the maxima (and minima) of the oscillations in the x direction are spaced ≈ 20.0 units apart.

In the Table below, we provide the values of the critical sensing radius $\rho_c(\lambda)$ as a function of λ. We also provide, as a function of λ, the spacing of the maxima (and minima) $\rho_s(\lambda)$ of the density functions as they oscillate, at the critical sensing radius values $\rho_c(\lambda)$. Both $\rho_c(\lambda)$ and $\rho_s(\lambda)$ are decreasing functions of the force of adhesion parameter λ. In Figure 15 we graph $\rho_c(\lambda)$ and $\rho_s(\lambda)$.

Table 1. Values of the critical sensing radius $\rho_c(\lambda)$ as a function of λ, and values of the spacing $\rho_s(\lambda)$ in the cell density function at the critical value $\rho_c(\lambda)$, as a function of λ.

λ	4.5	5.0	5.5	6.0	6.5	7.0	7.5	8.0	8.5	9.0	9.5	10.0
$\rho_c(\lambda)$	26.0	17.0	13.0	11.0	9.2	8.0	7.0	6.5	6.25	6.0	5.5	5.0
$\rho_s(\lambda)$	50.0	38.5	31.0	27.8	22.2	20.0	17.5	16.3	15.7	15.3	14.5	13.0

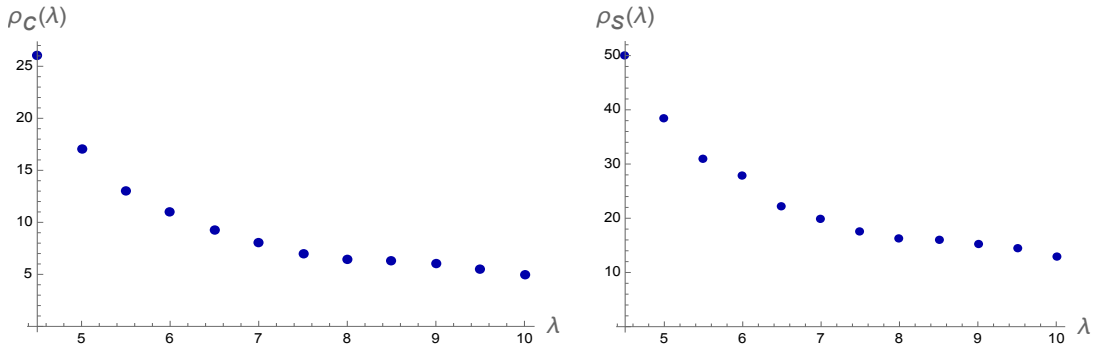

Figure 15. Left side: Graph of the critical sensing radius $\rho_c(\lambda)$; Right side: Graph of the spacing of the oscillations $\rho_s(\lambda)$ of the density function at the critical sensing radius.

4. Conclusions

A model of wound healing experiments has been investigated, based on the model (2.1) in [11]. A theoretical analysis was given in [11] for the existence, regularity, and boundedness of solutions of (2.1). Additionally, a sufficient condition on the parameters was established, for the convergence of solutions $n(x,t)$ to the complete wound free equilibrium $\bar{n}(x) \equiv 1.0$, as time advances.

In this work, the connection between the force of adhesion $g(n) = n(\lambda - n)$ and the sensing radius of cells ρ, is investigated for this model. Numerical simulations were given to connect the sensing radius ρ to the force of adhesion parameter λ, with the model parameters $\alpha = 1.0$ and initial condition $n_0(x) = 1.0 - 0.75\, e^{-(0.1x)^6}$. These numerical simulations demonstrate that for each $\lambda \in [4.5, 10.0]$, there is a critical value $\rho_c(\lambda)$ of the sensing radius, such that complete wound closure occurs for $\rho < \rho_c(\lambda)$ and incomplete wound closure occurs for $\rho > \rho_c(\lambda)$. This critical value $\rho_c(\lambda)$ is graphed in Figure 15 and decreases as λ increases. For $\lambda \leq 4.0$, the numerical simulations demonstrate that the wound closes for every value of the sensing radius ρ.

The result in [11] providing sufficient conditions on the sensing radius ρ to yield complete wound healing gives values considerably lower than the critical sensing radius $\rho_c(\lambda)$ for the numerical simulations for $\lambda = 5.0, 6.0, 7.0$. A complete theoretical establishment of necessary and sufficient conditions for the asymptotic stability of the equilibrium $n(x,t) \equiv 1$, $t \geq 0$, corresponding to complete wound closure in (2.1), remains an open problem.

The simulations also demonstrate the character of the ridges formed in incomplete closure, as time advances, with respect to their oscillation spacing. This oscillation spacing value $\rho_s(\lambda)$ is also graphed in Figure 15 and decreases as λ increases. These numerical simulations demonstrate the value of the cell–cell adhesion model (2.1) for understanding the output of wound healing experiments, which are of major importance in medical research of therapies for human diseases. The numerical simulations were carried out using MATHEMATICA and are available upon request.

Conflict of interest

The author declares there is no conflicts of interest.

References

1. M. Basan, J. Elgeti, E. Hannezo, W. J. Rappel, H. Levine, Alignment of cellular motility forces with tissue flow as a mechanism for efficient wound healing, *Proc. Natl. Acad. Sci.*, **110** (2013), 2452–2459. https://doi.org/10.1073/pnas.1219937110
2. H. Byrne, M. A. J. Chaplain, D. L. Evans, I. Hopkinson, Mathematical modelling of angiogenesis in wound healing: Comparison of theory and experiment, *J. Theor. Med.*, **2** (2000), 175–197. https://doi.org/10.1080/10273660008833045
3. G. J. Doherty, H. T. McMahon, Mediation, modulation and consequences of membrane-cytoskeleton interactions, *Ann. Rev. Biophys.*, **37** (2008), 65–95. https://doi.org/10.1146/annurev.biophys.37.032807.125912
4. J. Jonkman, J. Cathcart, F. Xu, M. Bartolini, J. Amon, K. Stevens, et al., An introduction to the wound healing assay using live-cell microscopy, *Cell Adh. Migr.*, **8** (2014), 440–451. https://doi.org/10.4161/cam.36224
5. S. Kauanova, A. Urazbayev, I. Vorobjev, The frequent sampling of wound scratch assay reveals the "opportunity" window for quantitative evaluation of cell motility-impeding drugs, *Front. Cell Dev. Biol.*, **11** (2021), 391. https://doi.org/10.3389/fcell.2021.640972
6. D. L. Nikolic, A. N. Boettiger, D. Bar-Sagi, J. D. Carbeck, S. Y. Shvartsman, Role of boundary conditions in an experimental model of epithelial wound healing, *Am. J. Physiol. Cell Physiol.*, **291** (2006), C68–C75. https://doi.org/10.1152/ajpcell.00411.2005
7. J. O′Connor, A. Stevens, E. Shannon, F. Akbar, K. LaFever, N. Narayanan, et al., Proteolytic activation of Growth-blocking peptides triggers calcium responses through the GPCR Mthl10 during epithelial wound detection, *Dev. Cell*, **56** (2021), 2160–2175. https://doi.org/10.1016/j.devcel.2021.06.020
8. J. S. Ross, J. A. Fletcher, G. P. Linette, J. Stec, E. Clark, M. Ayers, et al., The Her-2/neu gene and protein in breast cancer 2003: biomarker and target of therapy, *Oncologist*, **8** (2003), 307–325. https://doi.org/10.1634/theoncologist.8-4-307
9. A. Tremel, A. Cai, N. Tirtaatmadja, B. D. Hughes, G. W. Stevens, K. A. Landman, et al., Cell migration and proliferation during monolayer formation and wound healing, *Chem. Eng. Sci.*, **64** (2009), 247–253. https://doi.org/10.1016/j.ces.2008.10.008
10. S. E. Wang, P. Hinow, N. Bryce, A. M. Weaver, L. Estrada, C. L. Arteaga, et al., A mathematical model quantifies proliferation and motility effects of TGF–β on cancer cells, *Comput. Math. Methods Med.*, **10** (2009), 71–83. https://doi.org/10.1080/17486700802171993
11. J. Dyson, S. Gourley, R. Villella-Bressan, G. Webb, Existence and asymptotic properties of solutions of a nonlocal evolution equation modelling cell-cell adhesion, *SIAM J. Math. Anal.*, **42** (2010), 1784–1804. https://doi.org/10.1137/090765663
12. J. C. Arciero, Q. Mi, M. F. Branco, D. J. Hackam, D. Swigon, Continuum model of collective cell migration in wound healing and colony expansion, *Biophys. J.*, **100** (2011), 535–543. https://doi.org/10.1016/j.bpj.2010.11.083
13. N. J. Armstrong, K. J. Painter, J. A. Sherratt, A continuum approach to modelling cell-cell adhesion, *J. Theor. Biol.*, **243** (2006), 98–113. https://doi.org/10.1016/j.jtbi.2006.05.030

14. N. J. Armstrong, K. J. Painter, J. A. Sherratt, Adding adhesion to a chemical signalling model for somite formation, *Bull. Math. Biol.*, **71** (2009), 1–24. https://doi.org/10.1007/s11538-008-9350-1

15. V. Bitsouni, M. A. J. Chaplain, R. Eftimie, Mathematical modelling of cancer invasion: the multiple roles of TGF-β pathway on tumour proliferation and cell adhesion, *Math. Mod. Meth. Appl. Sci.*, **27** (2017), 1929–1962. https://doi.org/10.1142/S021820251750035X

16. H. Byrne, M. A. J. Chaplain, Modelling the role of cell-cell adhesion in the growth and development of carcinomas, *Math. Comput. Model.*, **24** (1996), 1–17. https://doi.org/10.1016/S0895-7177(96)00174-4

17. H. Byrne, D. Draso, Individual based and continuum models of growing cell populations: A comparison, *J. Math. Biol.*, **58** (2009), 657–687. https://doi.org/10.1007/s00285-008-0212-0

18. X. Chen, A. Friedman, A free boundary problem arising in a model of wound healing, *SIAM J. Math. Anal.*, **32** (2000), 778–800. https://doi.org/10.1137/S0036141099351693

19. V. Christini, J. Lowengrub, *Multi-Scale Modeling of Cancer*, Cambridge University Press, 2010. https://doi.org/10.1017/CBO9780511781452

20. P. D. Dale, P. K. Maini, J. A. Sherratt, Mathematical modeling of corneal epithelial wound healing, *Math. Biosci.*, **124** (1994), 127–147. https://doi.org/10.1016/0025-5564(94)90040-X

21. P. D. Dale, J. A. Sherratt, P. K. Maini, A mathematical model for collagen fibre formation during foetal and adult dermal wound healing, *Proc. Royal Soc. B*, **263** (1996), 653–660. https://doi.org/10.1098/rspb.1996.0098

22. J. C. Dallon, J. A. Sherratt, P.K. Maini, Modeling the effects of transforming growth factor–β on extracellular matrix alignment in dermal wound repair, *Wound Repair Regen.*, **9** (2001), 278–286. https://doi.org/10.1046/j.1524-475X.2001.00278.x

23. A. Ducrot, P. Magal, S. Ruan, Travelling wave solutions in multigroup age–structured epidemic models, *Arch. Ration Mech. Anal.*, **195** (2010), 311–331. https://doi.org/10.1007/s00205-008-0203-8

24. R. Durrett, Cancer modeling: A personal perspective, *Not. Am. Math. Soc.*, **60** (2013), 304–309. https://doi.org/10.1090/noti953

25. J. Dyson, S. Gourley, G. Webb, A nonlocal evolution equation model of cell-cell adhesion in higher dimensional space, *J. Biol. Dyn.*, **7** (2013), 68–87. https://doi.org/10.1080/17513758.2012.755572

26. J. Dyson, E. Sánchez, R. Villella-Bressan, G. Webb, An age and spatially structured model of tumor invasion with haptotaxis, *Discrete Contin. Dyn. Syst. Ser. –B*, **8** (2007), 45–60. https://doi.org/10.3934/dcdsb.2007.8.45

27. J. Dyson, R. Villella-Bressan, G. Webb, A spatially structured model of tumor growth with cell age, cell size and mutation of cell phenotypes, *Math. Model. Nat. Phenom.*, **2** (2007), 69–100. https://doi.org/10.1051/mmnp:2007004

28. J. Dyson, R. Villella-Bressan, G. Webb, An age and spatially structured model of tumor invasion with haptotaxis II, *Math Popul. Stud.*, **15** (2008), 73–95. https://doi.org/10.1080/08898480802010159

29. J. Dyson, R. Villella-Bressan, G. Webb, Global existence and boundedness of solutions to a model of chemotaxis, *Math. Model. Nat. Phenom.*, **3** (2008), 17–35. https://doi.org/10.1051/mmnp:2008039

30. J. Dyson, G. Webb, A cell population model structured by cell age incorporating cell–cell adhesion, *Mathematical Oncology*, Birkhauser, New York, NY, 2014, 109–149. https://doi.org/10.1007/978-1-4939-0458-7_4

31. A. Friedman, Tutorials in Mathematical Biosciences, II: Cell Cycle, Proliferation, and Cancer, *Springer Lecture Notes in Mathematics*, **1872**, (2005). https://doi.org/10.1007/978-3-319-08314-8

32. A. Friedman, Mathematical analysis and challenges arising from models of tumor growth, *Math. Mod. Meth. Appl. Sci.*, **17** (2007), 1751–1772. https://doi.org/10.1142/S0218202507002467

33. A. Friedman, B. Hu, C. Xue, Analysis of a mathematical model of ischemic cutaneous wounds, *SIAM J. Math. Anal.*, **42** (2010), 2013–2040. https://doi.org/10.1137/090772630

34. X. Fu, Q. Griette, P. Magal, Existence and uniqueness of solutions for a hyperbolic Keller-Segel equation, *Discrete Contin. Dyn. Syst. Ser. B*, **26** (2021), 1931–1966. https://doi.org/10.3934/dcdsb.2020326

35. E. A. Gaffney, P. K. Maini, J. A. Sherratt, P. D. Dale, Wound healing in the corneal epithelium: biological mechanisms and mathematical models, *J. Theor. Med.*, **1** (1997), 13–23. https://doi.org/10.1080/10273669708833003

36. E.A. Gaffney, P. K. Maini, J.A. Sherratt, S. Tutt, The mathematical modelling of cell kinetics in corneal epithelial wound healing, *J. Theor. Biol.*, **197** (1999), 111–141. https://doi.org/10.1006/jtbi.1998.0852

37. A. Gandolfi, M. Iannelli, G. Marnoschi, An age-structured model of epidermis growth, *J. Math. Biol.*, **62** (2011), 111–141. https://doi.org/10.1007/s00285-010-0330-3

38. A. Gandolfi, M. Iannelli, G. Marinoschi, Time evolution for a model of epidermis growth, *J. Evol. Equ.*, **13** (2013), 509–533. https://doi.org/10.1007/s00028-013-0188-0

39. A. Gerisch, M. A. J. Chaplain, Mathematical modelling of cancer cell invasion of tissue: local and nonlocal models and the effect of adhesion, *J. Theor. Biol.*, **250** (2008), 684–704. https://doi.org/10.1016/j.jtbi.2007.10.026

40. D. Guidetti, On elliptic systems in L^1, *Osaka J. Math.*, **30** (1993), 397–429.

41. J. S. Lowengrub, H. B. Frieboes, F. Jin, Y-L. Chuang, X. Li, P. Macklin, et al., Nonlinear models of cancer: Bridging the gap between cells and tumours, *Nonlinearity*, **23** (2010), R1–R91. https://doi.org/10.1088/0951-7715/23/1/R01

42. S. McDougall, J. Dallon, J.A. Sherratt, P. Maini, Fibroblast migration and collagen deposition during dermal wound healing: mathematical modelling and clinical implications, *Philos. Trans. Royal Soc. A*, **364** (2006), 1385–1405. https://doi.org/10.1098/rsta.2006.1773

43. P. J. Murray, J. W. Kang, G. R. Mirams, S. Y. Shin, H. M. Byrne, P. K. Maini, et al., Modelling spatially regulated β-catenin dynamics and invasion in intestinal crypts, *Biophys. J.*, **99** (2010), 716–725. https://doi.org/10.1016/j.bpj.2010.05.016

44. P. J. Murray, A. Walter, A. G. Fletcher, C. M. Edwards, M. J. Tindall, P. K. Maini, Comparing a discrete and continuum model of the intestinal crypt, *Phys. Biol.*, **8** (2010), 026011. https://doi.org/10.1088/1478-3975/8/2/026011

45. L. Olsen, J. A. Sherratt, P. K. Maini, A mechanochemical model for adult dermal wound contraction and the permanence of the contracted tissue displacement profile, *J. Theor. Biol.*, **14** (1997), 261–281. https://doi.org/10.1093/imammb/14.4.261

46. L. Olsen, J. A. Sherratt, P. K. Maini, F. Arnold, A mathematical model for the capillary endothelial cell-extracellular matrix interactions in wound-healing angiogenesis, *Math. Med. Biol.*, **14** (1997), 261–281. https://doi.org/10.1093/imammb/14.4.261

47. M. Owen, J. A. Sherratt, Pattern formation and spatiotemporal irregularity in a model for macrophage-tumour interactions, *J. Theor. Biol.*, **189** (1997), 63–80. https://doi.org/10.1006/jtbi.1997.0494

48. K. J. Painter, N. J. Armstrong, J. A. Sherratt, The impact of adhesion on cellular invasion processes in cancer and development, *J. Theor. Biol.*, **264** (2010), 1057–1067. https://doi.org/10.1016/j.jtbi.2010.03.033

49. K. J. Painter, J. A. Sherratt, Modelling the movement of interacting cell populations, *J. Theor. Biol.*, **225** (2003), 327–339. https://doi.org/10.1016/S0022-5193(03)00258-3

50. J. Pasquier, P. Magal, C. Boulange-Lecomte, G. Webb, F. Le Foll, Consequences of cell-to-cell P–glycoprotein transfer on acquired multidrug resistance in breast cancer: a cell population dynamics model, *Biol. Direct*, **6** (2011), 1–18. https://doi.org/10.1186/1745-6150-6-5

51. G. J. Pettet, M. A. J. Chaplain, D. S. L. McElwain, H. M. Byrne, On the role of angiogenesis in wound healing, *Proc. Roy. Soc. Lond. B*, **263** (1996), 1487–1493. https://doi.org/10.1098/rspb.1996.0217

52. G. J. Pettet, M. A. J. Chaplain, D. S. L. McElwain, J. Norbury, A model of wound healing-angiogenesis in soft tissue, *Math. Biosci.*, **136** (1996), 35–63. https://doi.org/10.1016/0025-5564(96)00044-2

53. J. A. Sherratt, M. A. J. Chaplain, A new mathematical model for avascular tumour growth, *J. Math. Biol.*, **43** (2001), 291–312. https://doi.org/10.1007/s002850100088

54. J. A. Sherratt, J. C. Dallon, Theoretical models of wound healing: past successes and future challenges, *C. R. Biol.*, **325** (2002), 557–564. https://doi.org/10.1016/S1631-0691(02)01464-6

55. J. A. Sherratt J. D. Murray, Mathematical analysis of a basic model for epidermal wound healing, *J. Math. Biol.*, **29** (1991), 389–404. https://doi.org/10.1007/BF00160468

56. J. A. Sherratt, S. A. Gourley, N. J. Armstrong, K. J. Painter, Boundedness of solutions of a nonlocal reaction-diffusion model for adhesion in cell aggregation and cancer invasion, *Eur. J. Appl. Math.*, **20** (2009), 123–144. https://doi.org/10.1017/S0956792508007742

57. J. A. Sherratt, J. D. Murray, Models of epidermal wound healing, *J. Math. Biol.*, **31** (1993), 703–716. https://doi.org/10.1007/BF00160420

58. C.M. Topaz, A. L. Bertozzi, M. A. Lewis, A nonlocal continuum model for biological aggregation, *Bull. Math Biol.*, **68** (2006), 1601–1623. https://doi.org/10.1007/s11538-006-9088-6

59. S. Turner, J. A. Sherratt, Intercellular adhesion and cancer invasion: a discrete simulation using the extended Potts model, *J. Theor. Biol.*, **216** (2002), 85–100. https://doi.org/10.1006/jtbi.2001.2522

60. S. Turner, J. A. Sherratt, D. Cameron, Tamoxifen treatment failure in cancer and the nonlinear dynamics of TGFβ, *J. Theor. Biol.*, **229**(2004), 101–111. https://doi.org/10.1016/j.jtbi.2004.03.008

61. Ch. Walker, Global well–posedness of a haptotaxis model with spatial and age structure, *Differ. Integral Equ.*, **20** (2007), 1053–1074.

62. Ch. Walker, A Haptotaxis model with age and spatial structure and nonlinear age-boundary conditions, *Proc. Appl. Math.*, **7** (2007), 1040601–1040602. https://doi.org/10.1002/pamm.200700008

63. Ch. Walker, Global existence for an age and spatially structured haptotaxis model with nonlinear age-boundary conditions, *Eur. J. Appl. Math.*, **19** (2008), 113–147. https://doi.org/10.1017/S095679250800733X

64. H.J. Wearing, J. A. Sherratt, Keratinocyte growth factor signalling: a mathematical model of dermal–epidermal interaction in epidermal wound healing, *Math. Biosci.*, **165** (2000), 41–62. https://doi.org/10.1016/S0025-5564(00)00008-0

65. C. Xue, A. Friedman, C. K. Sen, A mathematical model of ischemic cutaneous wounds, *Proc. Nat. Acad. Sci. USA*, **106** (2009), 16782–16787. https://doi.org/10.1073/pnas.0909115106

AIMS Press